13

Influence of Sintering Temperature on Magnetotransport Behavior of Some Nanocrystalline Manganites

G. Venkataiah[2], Y. Kalyana Lakshmi[1] and P. Venugopal Reddy[1,*]
[1]*Department of Physics, Osmania University, Hyderabad,*
[2]*Materials and Structures Laboratory, Tokyo Institute of Technology,*
Nagatsuta, Midori-ku, Yokohama,
[1]*India*
[2]*Japan*

1. Introduction

The colossal magnetoresistance (CMR) in hole doped manganese oxides, widely known as manganites with formula $Ln_{1-x}Ae_xMnO_3$ (where Ln is a trivalent rare earth and Ae is a divalent alkaline earth ion; x=0-1), has been intensively studied over the last two decades. In general, these systems comprise a strong competition between charge, orbital, lattice and spin degrees of freedom all of which make them an intriguing subject of research (Dogotto, 2003; Goodenough, 2003; Ramirez, 1997; Tokura, 2000). The end-members of this system are antiferromagnetic (AFI) insulators. Partial substitution of the Ln with divalent alkaline-earth ion of the ABO_3 structure introduces mixed valence Mn^{4+}/Mn^{3+} on the B site. With decreasing temperature the system undergoes a transition from the paramagnetic to the ferromagnetic state accompanied by a metal-insulator transition. A large number of studies on CMR materials of different forms such as single crystals (Okuda et al., 1998; Zhou et al., 1997), thin film (Kwon et al., 1997; Rao et al., 1998; Suzuki et al., 1997) and ceramics (Hwang et al., 1995; Mahendiran et al., 1996a, 1996b) for the basic research point of view and also the possible future device applications view point. The Zener (1951) has proposed a simplest model, known as double-exchange (DE) model to explain the electrical behavior in ferromagnetic metallic region below Curie Temperature (T_C). However, due to various interactions among charge, spin and lattice makes these materials more complex and DE alone cannot explain the entire electrical transport behavior. Later on various theoretical models have been proposed by considering, electron-lattice and spin lattice interaction and even today there is no comprehensive model to explain transport phenomena in manganites (Millis et al., 1995; Tokura, 2000).

These doped perovskite manganites show large magnetoresistance (MR) around metal to insulator transition temperature (T_P) at high magnetic fields and below room temperatures which restricts their applicability to hands on devices. Improved MR could be achieved for

* Corresponding Author

nanosized perovskite manganite samples prepared through the sol–gel process. The sol–gel process also has potential advantages over other traditional processing techniques such as better homogeneities, low processing temperature and improved material properties. Although there are several reports on the synthesis of nanoscale manganites, none of them were carried out systematically in the context of the influence of sintering temperature on the electrical, magnetic and magneto transport behavior of manganites. It is well know that when the size of the particles is reduced to a few nanometers some of the basic properties such as magnetoresistance, superparamagnetism, coercivity, Curie temperature and Saturation magnetization are effected when compared with their bulk counterparts. Several works on different nanoscale systems indicate that the surface is responsible for their apparent anomalous behavioral changes with reduced dimensions. In fact, the preparation procedure and sintering conditions determines the nature of the surface region of nanosize grains, which plays a very crucial role in electrical transport, magnetic, and magnetotransport behavior of nano dimensional systems. Therefore, it is felt that a detailed review on the influence of sintering on magnetotransport behavior of manganites is essential and important.

The senior author of the paper (P. V. Reddy) along with his group of students investigated the structural, magnetic, electrical and magnetotransport properties of a number doped manganites over a period of more than a decade and published a series of papers in a number of International Journals (Kalyana Lakshmi and Reddy 2008, 2009a, 2009b, 2010, 2011; Kalyana Lakshmi et al., 2009; Venkataiah et al., 2005, 2007a, 2007b, 2007c, 2008, 2010; Venkataiah and Reddy, 2005, 2009a, 2009b). A summary of the work based on the influence of sintering on various properties of the manganites substituted with both divalent and monovalent ions is presented here.

2. Experimental procedure

The samples with different particle sizes were prepared using sol-gel route followed by heat treatment at four different sintering temperatures (T_S) (Venkataiah et al., 2005, 2007, 2008, 2010; Venkataiah and Reddy 2005, 2009a, 2009b; Kalyana Lakshmi and Reddy 2009a). Five series of samples i.e., $La_{0.67}Ca_{0.33}MnO_3$, $La_{0.67}Sr_{0.33}MnO_3$, $La_{0.67}Ba_{0.33}MnO_3$, $Nd_{0.67}Sr_{0.33}MnO_3$ and $La_{0.67}Na_{0.33}MnO_3$ were prepared to study the effect of sintering temperature on various properties. The samples are hereafter designated as LCMO, LSMO, LBMO, NSMO and LNMO respectively and the samples sintered at 800, 900, 1000 and 1100 C are designated with 8, 9, 10 and 11 numerical representations followed by compositional abbreviations. The synthesis procedure of sol-gel method is outlined in Fig. 1.

The stoichiometric amounts of oxides / carbonates were taken and all of them were converted into metal nitrates and the resultant nitrate mixture solution was converted into citrate by adding 1:1 ratio of the citric acid to the metal atoms present in the composition. To carry out the reaction at greater speed, a proper reaction environment is to be created and hence pH of the solution was adjusted between 6.5 and 7 by adding ammonia solution. Finally, the powder was pressed into pellets and sintered in air at four different temperatures i.e., 800, 900, 1000 and 1100^0C for 4 hr. For a direct comparison of the properties of the samples as a function of sintering temperature (grain size) it is important to ensure that the Mn^{4+} concentration remains similar in different samples, since it is

crucial factor in controlling the transport and magnetic properties. Mn^{4+} concentration has been determined by redox titrations (Vogel, 1978). The phase purity of the samples was checked by X-ray diffraction (XRD) and grain distribution was estimated by scanning electron microscopy (SEM). The electrical resistivity and magnetoresistance studies were undertaken by a Janis "supervaritemp" cryostat in applied fields of 0–7 T, over a temperature range of 77–300 K using a four-point probe method. a.c susceptibility measurements were carried out using a dual channel lock-in amplifier, while thermoelectric power studies were carried out by a two-probe differential method over a temperature range 77–300 K.

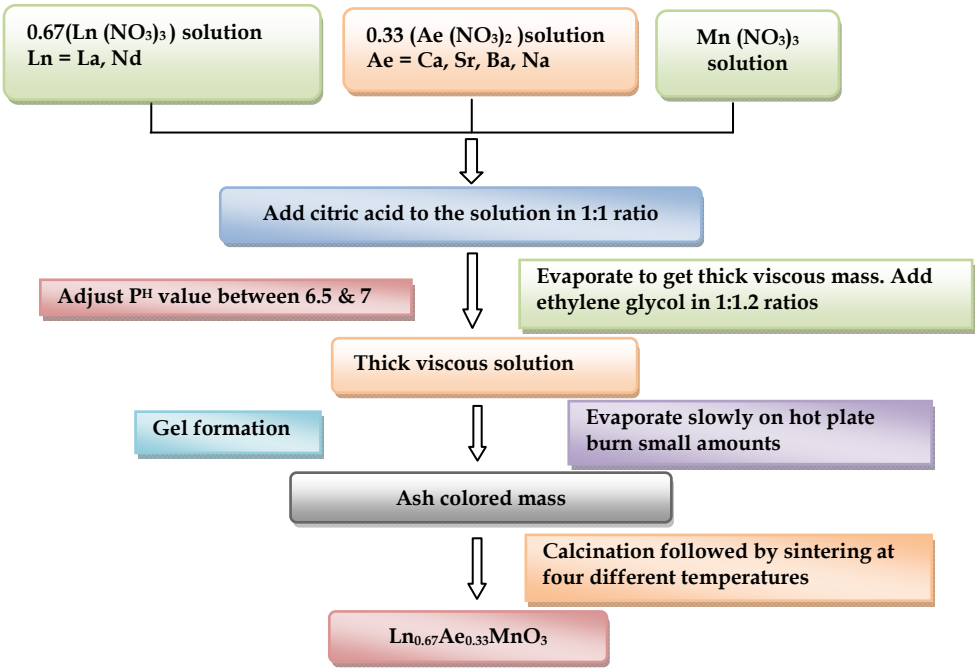

Fig. 1. A flow chart of Sol-gel method for the preparation of CMR manganites.

3. Results & discussions

3.1 Structural properties

Most of the manganites crystallize in the various derivatives of the so-called perovskites structure named after the mineral perovskite, $CaTiO_3$.Figure 2 illustrates the ideal cubic perovskite structure, with the general formula ABO_3. The structure may be conceived as a close-packed array formed of O^{2-} anions and A cations with B cations located at the

octahedral interstitial sites. The BO_6 octahedra make contact to each other by their vertices and form a three-dimensional network. In manganites the A-sites of the perovskite structure are occupied by trivalent rare earth ion while B-sites with Mn ions. The stability of the perovskite structure depends strongly on the size of the A-site and B-site ions. If there is a size mismatch between the A-site and B-site ions and the space in the lattice where they reside, the perovskite structure will become distorted. Such a lattice distortion of perovskite structure is governed by Goldschmidt's tolerance factor (τ) (Goldschmidt, 1953).

$$\tau = (r_A + r_O)/\sqrt{2}(r_B + r_O) \quad (1)$$

where r_A and r_B are the mean radii of the ions occupying the A-sites and B-sites, respectively, and r_O is the ionic radius of oxygen. For an ideal cubic perovskite τ=1.

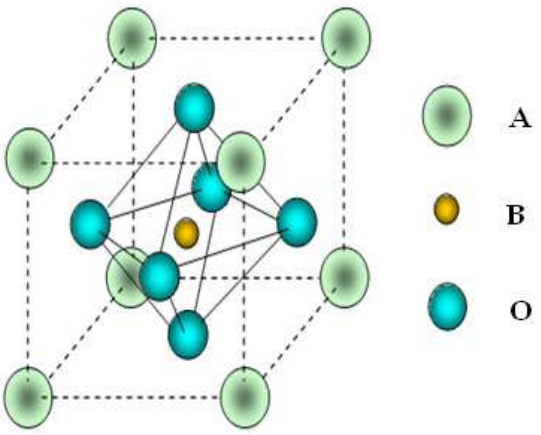

Fig. 2. Unit cell structure of prototype cubic perovskite, ABO_3, with A ions situated at the corners, B ions in the center and oxygen ions at the centers of the faces.

If τ differs slightly from unity the atoms are displaced from their ideal positions to minimize the free energy and a distorted perovskite structure is formed. For $0.96<\tau<1$ the lattice structure transforms to the rhombohedral structure and then to orthorhombic structure for $\tau<0.96$, in which B-O-B bond angle gets distorted from 180°. Structure like tetragonal, hexagonal and monoclinic etc. are reported for manganites for different x values. Among the studied samples the LSMO, LBMO and LNMO systems crystallize in the rhombohedral with $R\ \bar{3}c$ space group (Venkataiah et al., 2007a, 2010; Kalyana Lakshmi and Reddy 2009a) while LCMO and NSMO group of samples crystallize in to orthorhombic structure with *Pbnm* space group (Venkataiah et al., 2005; Venkataiah and Reddy 2009b). A typical XRD patterns of LSMO & NSMO samples are shown in Figure 3. The X-ray linewidths are used to estimate average crystallite size <s> values through the Scherrer's formula modified by Williamson and Hall (1953).

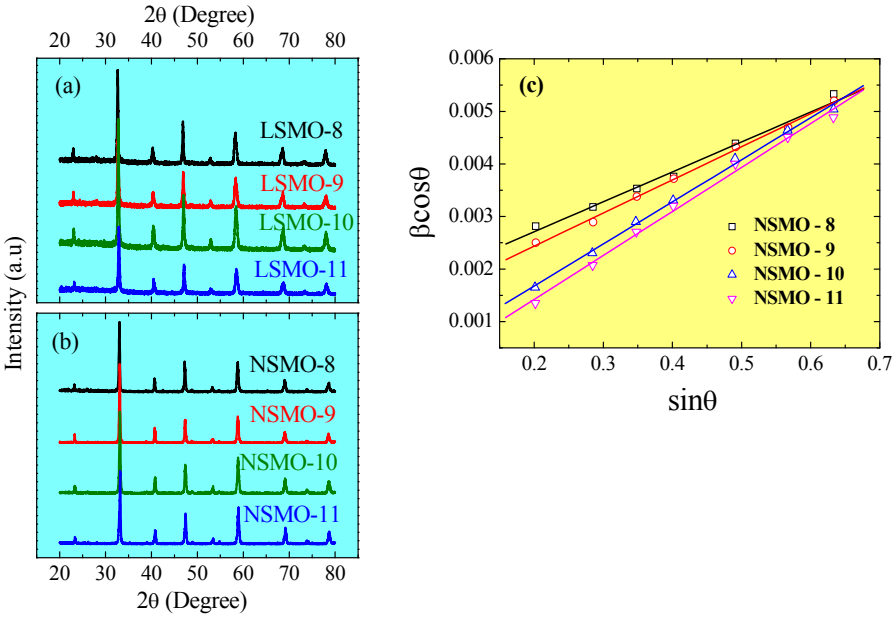

Fig. 3. (a, b) XRD patterns of LSMO & NSMO group of manganites at various sintering temperatures (T_S) (c) Williamson-Hall plot of $Nd_{0.67}Sr_{0.33}MnO_3$ manganites.

In this method, the experimental x-ray peak broadening is given by $\beta=\varepsilon\tan\theta+K\lambda/ st\cos\theta$, where β is the full width at half maximum (FWHM) of the XRD peaks after subtracting FWHM of the standard sample (SiO_2), θ is the Bragg angle, K is the grain shape factor (0.89), λ is the wavelength of Cu Kα radiation, and ε is the strain in the sample. A plot between βcosθ versus sinθ is shown in Figure 3(c). The average crystallite sizes were calculated from the intercept of the straight line with the vertical axis, while the slope of the line gives the lattice strain (ε). The average crystallite sizes are found to increase with increasing sintering temperature and are in nanometer range. The variation of crystallite size with sintering temperature is shown in Figure 4. In fact, the computed crystallite sizes are comparable with those obtained from SEM. Figure 5 shows the representative SEM images of LSMO samples sintered at 800 and 1100ºC. The SEM observation reveals that there is a uniform distribution of grain sizes for the samples and as the sintering temperature increases, the grain size increases and porosity decreases.

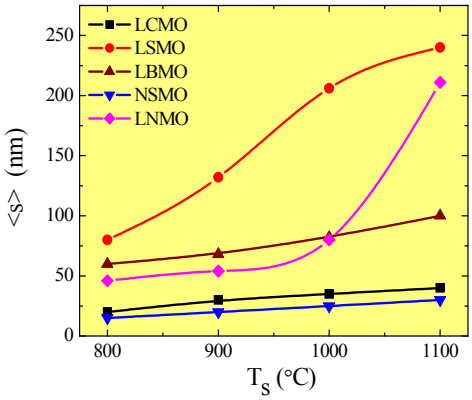

Fig. 4. Variation of Crystallite size (<s>) in nanometers with Sintering temperature (T_S °C).

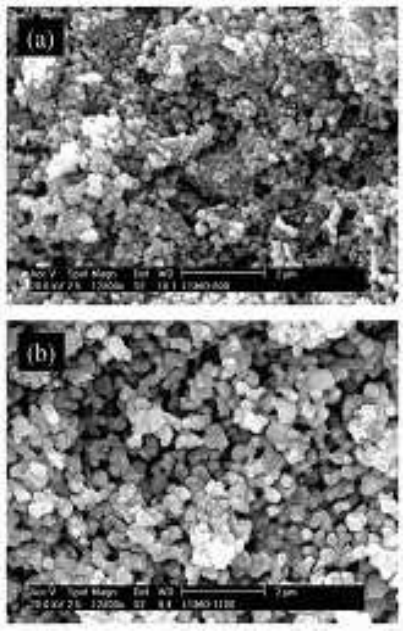

Fig. 5. SEM images of LSMO samples sintered at 800 & 1100°C.

3.2 Magnetic properties

Mixed-valence manganites are complex materials showing a rich variety of structural, magnetic and electronic phases. Phase transitions may be induced by changing the composition, temperature or sometimes by applying an external magnetic field. Usually

structural, magnetic and electronic phase transitions occur simultaneously. The magnetic and electronic properties of lanthanum manganites, $La_{1-x}Ae_xMnO_3$ (Ae = Ca, Sr, etc) are strongly related to the simultaneous presence of manganese in different valence states. The end-members, $x = 0$ and $x = 1$, containing Mn in only one valence state (for divalent ion at A-site substitution leads to Mn in 3+ and 4+ valence states), are usually antiferromagnetic insulators (AFI), but intermediate compositions, which have mixed Mn valence, may be ferromagnetic and have good conducting properties. Figure 6 illustrates the magnetic and electrical properties of $La_{1-x}Ca_xMnO_3$ (x=0-1) system with change in composition and temperature (Schiffer et al., 1995, Urushibara et al., 1995). Ferromagnetic behavior starts to manifest itself when x is 0.1 and the composition upto x~0.3 have both antiferromagnetic (AFM) and ferromagnetic (FM) characteristics. The x=0.3 composition is clearly FM, while the x>0.5 compositions are AFM. The coexistence of metallic conductivity and ferromagnetic coupling in these materials at low temperature has been explained in terms of a double exchange mechanism, proposed by Zener in 1951. The double exchange mechanism involves simultaneous transfer of an electron from Mn^{3+} to O^{2-} and from O^{2-} to Mn^{4+}. Moreover, the properties of manganites are not only sensitive to the manganese valency, but also are strongly affected by other factors such as average cationic radius $\langle r_A \rangle$ of A-site and A-site cationic mismatch quantified by σ^2 which effects the magnetic interaction. Due to the long history of work on these compounds, most of the studies have been performed on bulk ceramics and thin films. Apart from this it was demonstrated that the properties of manganites are strongly affected by particle size. It was found that the sintering temperature is one of the key factors which influences the crystallization and microstructure of the perovskite samples. The basic magnetic properties such as spontaneous magnetization, the Curie temperature and coercivity are strongly influenced with sintering temperature. Mahesh et al., (1996) were the first to explore the size effects in polycrystalline $La_{0.67}Ca_{0.33}MnO_3$prepared by citrate-gel route and observed a close relationship between magnetotransport properties and microstructure.

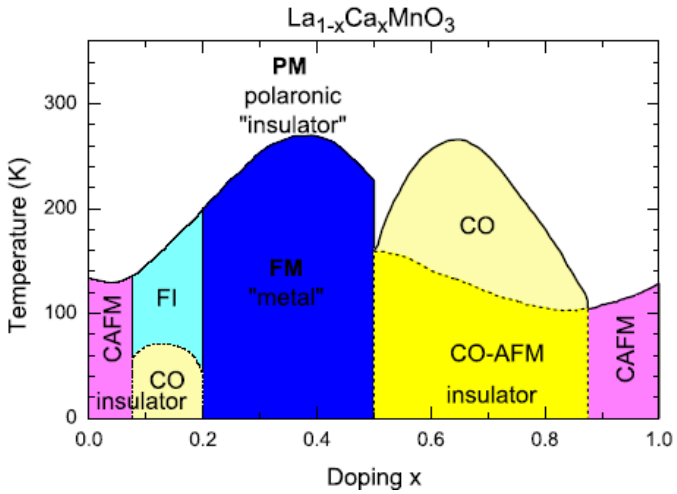

Fig. 6. Magnetic and electronic phase diagram versus doping x for $La_{1-x}Ca_xMnO_3$ manganites (Schiffer et al., 1995, Urushibara et al., 1995).

The results obtained by the authors of the present investigation on five series of samples sintered at various temperatures are presented in this section. Out of these samples, the a.c. susceptibility (χ) versus temperature plots of two representative samples viz., LSMO and LBMO sintered at different temperatures are displayed in Figure 7. All the five groups of samples exhibit para to ferromagnetic transition with decreasing temperature and the width of transition broadens on lowering sintering temperature indicating magnetic inhomogeneity in the samples. The variation of T_C with sintering temperature (T_S) for the samples is shown in Figure 8. T_C values do not vary much in the case of LSMO and LBMO systems (Venkataiah et al., 2007a, 2010) while after an initial increase they remain almost constant with further increase in sintering temperature for $La_{0.67}Na_{0.33}MnO_3$manganites (Kalyana Lakshmi & Reddy 2009a). The observed behavior may be explained qualitatively as follows. In general variations in T_C values take place whenever there is a change in Mn–O–Mn bond angle as well as Mn–O bond length, thereby indicating the presence of magnetic inhomogeneity in the sample as it approaches the transition temperature. In contrast to these arguments, perhaps due to magnetic homogeneity especially as sample approaches the phase transition, T_C might be remaining constant, thereby giving an impression that T_C might be independent of grain size. In fact a similar conclusion was arrived at earlier in the case of $La_{0.7}Sr_{0.3}MnO_3$ (Gaur & Verma 2006) and $La_{0.8}Ca_{0.2}MnO_3$ manganites (Balcells et al., 1998; Fu 2000; Rivas et al., 2000).

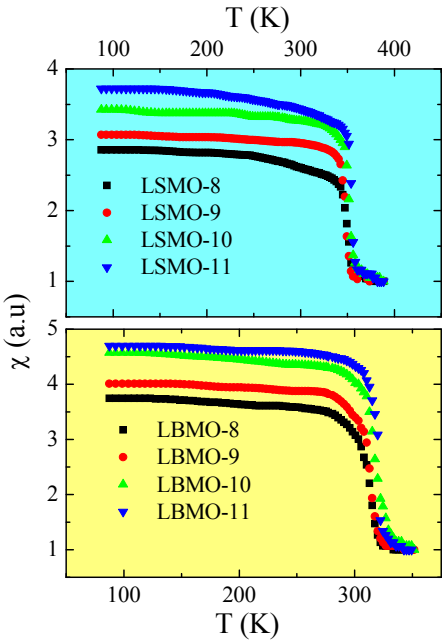

Fig. 7. Variation of susceptibility (χ) with temperature for (a) LSMO & (b) LBMO group of manganites.

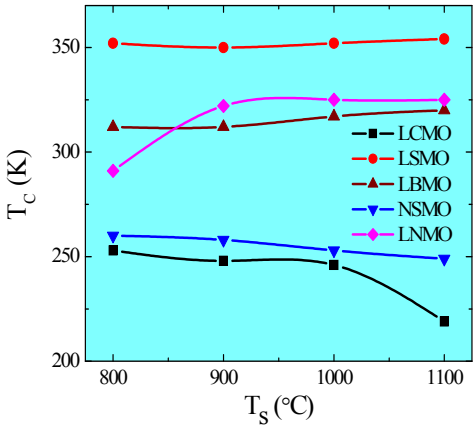

Fig. 8. Variation of Curie temperatures (T_C) as a function of sintering temperature (T_S).

In contrast to the above results, T_C values decrease with increasing sintering temperature in the case of LCMO and NSMO manganites (Venkataiah et al., 2005; Venkataiah & Reddy 2005). The observed reduction of ferromagnetic transition temperature (T_C) with increasing particle size is related to increase in unit cell volume. The increased unit cell volume enhances Mn–O bond length thereby deviating Mn–O–Mn bond angle from 180^0, which in turn decreases the overlap integral decreasing the bandwidth. Thus the lattice effects arising from increasing particle size are expected to decrease in bandwidth, which in turn decreases T_C. In addition, the dependence of T_C on <s> ($T_C \propto 1/ <s>$) can also be rationalized if the size reduction can be thought as producing an internal pressure (P_I) such as the hydrostatic pressure (P_E): Size reduction due to interface stress can lead to an internal pressure $\Delta P_I \propto A_g / V_g$, where A_g and V_g are the surface area and the volume of a nanocrystal respectively. For a nearly spherical particle, the relationship between A_g and V_g is given by a relation, $A_g / V_g \propto 1/ <s>$. This gives $\Delta P_I \propto 1/ <s>$. As per the external, hydrostatic pressure, $dT_C = dP_I \approx$ constant, one can write as $\Delta T_C \propto 1/ <s>$ (Shankar et al., 2004; Venkataiah and Reddy, 2009b).

3.3 Electrical studies

A fundamental characteristic of mixed-valence manganites is the close relationship between electronic transport and magnetism. Most of the $La_{1-x}Ae_xMnO_3$ compositions are paramagnetic insulators at room temperature and exhibit an increase in electrical resistivity with a decrease in temperature. Compositions that are ferromagnetic show insulating ($d\rho/dT < 0$) behavior above T_C, but the resistivity decreases with decreasing temperature, as in metals ($d\rho/dT > 0$), when they are cooled below T_C. This insulator-metal transition is therefore associated with a peak in resistivity at a temperature, T_P.

The variations of electrical resistivity with temperature for all the five groups of samples show similar behavior. The behavior of two representative samples viz., LCMO and LSMO

is shown in Figure 9. All the samples show metal to insulator transition at T_P and their variation with sintering temperature for the investigated samples is shown in Figure 10 (a). The metal to insulator transitions shifts towards low temperature side and the magnitude of resistivity increases on reducing the sintering temperature or particle size.These observations are in good agreements with those reported earlier (Mahesh et al., 1996; Gaur & Verma 2006). This behaviour can be explained by the core-shell model proposed by Zhang et al., (1997). In the core–shell structure the inner part of the grain, i.e. the core, would have the same properties as the bulk manganite, whereas the outer layer, i.e. the shell (thickness t), would contain most of the oxygen defects and crystallographic imperfections, which would lead to a magnetically disordered dead layer. As the surface to volume ratio becomes larger, i.e., the grain size is reduced, the shell thickness (t) increases. Basically, the net intercore barrier thickness (s = 2t + d), namely the total shell thickness (2t) of two neighboring grains together with the intergranular distance (d), increases with the reduction of grain size. Further, with the decrease in grain size, core separation (s ~ 2t) increases significantly with the thickness of the shell (t), even if we consider the grains to be in intimate contact (d = 0) for all grain size samples. Another important fact is that in the absence of magnetic field the contributory portion of each individual grain to the magnetization is the core and not

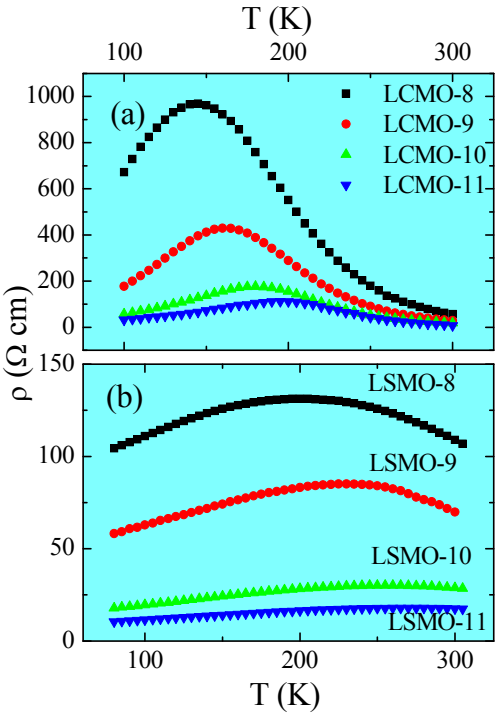

Fig. 9. Temperature dependence of resistivity for (a) LCMO & (b) LSMO samples sintered at various temperatures.

the shell, in the absence of applied magnetic field the net magnetization of the shell is considered to be zero. Since the surface would contain most of the oxygen defects and faults in the crystallographic structure that will lead to a magnetically disordered state, which may lead to formation of spin canting or antiferromagnetic state at the manganite grain surface, thereby decreasing T_P values and increasing the magnitude of resistivity (Figure 11).

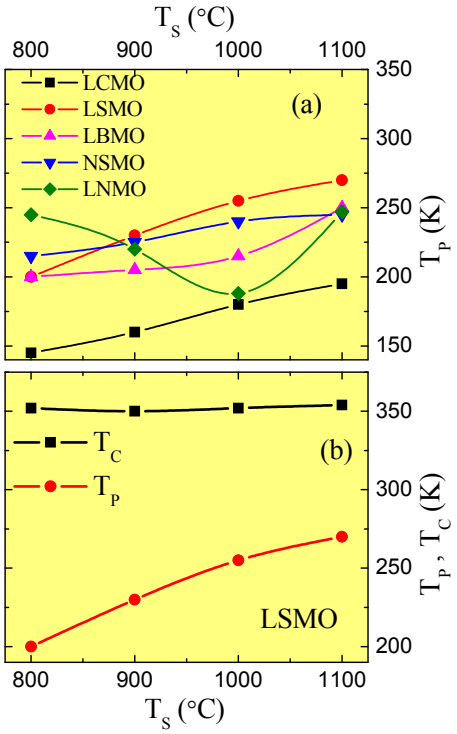

Fig. 10. (a) Variation of T_P (K) with sintering temperature (T_S) (b) T_C, T_P (K) variation of LSMO with T_S.

It can also be noticed from the Figure 10(b) (in the case of LSMO system) that there exists a large difference between T_C and T_P and the difference increases with decreasing sintering temperature. The large difference in the magnetic and electrical transitions for all the samples is thought to be due to the existence of the disorder and is in fact a common feature of the polycrystalline manganites (Gaur & Verma 2006). The T_C being an intrinsic characteristic does not show significant change as a function of sintering temperature. On the other hand T_P is an extrinsic property that strongly depends on the synthesis conditions and microstructure (e.g. grain boundary density). The suppression of the T_P as compared to T_C is caused by the induced disorders and also by the increase in the non-magnetic phase fraction, which is due to enhanced grain boundary densities as a consequence of lower sintering temperature. This also causes the increase in the carrier scattering leading to a corresponding enhancement in the resistivity. Thus lowering of sintering temperature reduces the metallic transition temperature and hence the concomitant increase in resistivity.

In contrast to the above results, it has been observed that T_P values of sodium doped samples, are found to decrease with increasing grain size except in the case of the sample sintered at 1100°C (Kalyana Lakshmi & Reddy, 2009a). The observed variation may be interpreted on the basis of oxygen deficiency. According to Malavasi et al., 2002, 2003a, 2003b) the presence of oxygen vacancies deeply affect the transport properties resulting in both Mn^{4+} reduction and point defect creation within the structure thereby shifting T_P towards low temperature side. This behavior is in close agreement with the results reported in the case of LCMO samples (Hueso et al., 1998) where T_C remained constant while T_P decreased with oxygen deficiency. This suggests that the combined effect of crystallite size and oxygen deficiency might be responsible for the observed resistivity behavior (Hueso et al., 1998; Malavasi et al., 2002, 2003a, 2003b).

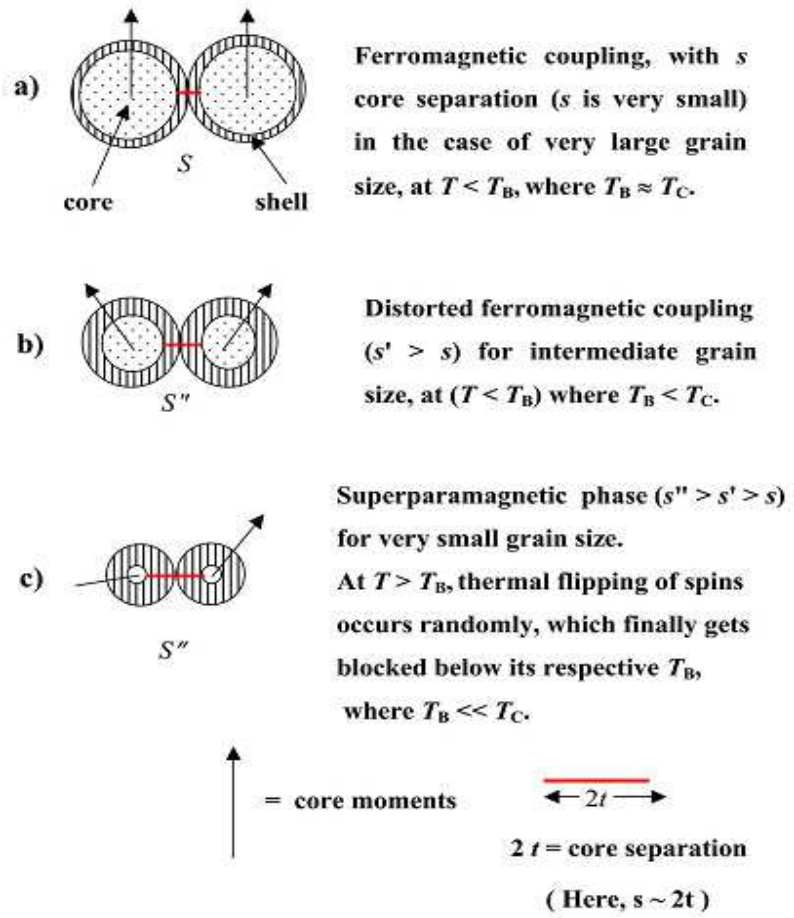

Fig. 11. Phenomenological demonstrative representation of the possible ordering of core moments in the core-shell structure of nanometric manganite grains with the grain size as a variable parameters in different temperature ranges [Dey and Nath 2006].

3.4 Thermopower studies

Measurement of emf (electromotive force) induced by a temperature gradient across a sample provides complementary information to the resisitivty. The Seebeck coefficient (S) is defined as $\Delta V/\Delta T$, the thermoelectric voltage per degree of temperature difference. Among various transport properties, thermopower is a simple and sensitive one for detecting the scattering mechanism that dominates the electronic conduction and also provides insight into changes of band structure near the metal-insulator transition. The thermoelectric power (TEP) of manganites shows strong temperature dependence and it can have positive or negative sign depending on the temperature and degree of substitution of divalent/monovalent cation that determines the carrier density in these systems. This behaviour suggests that either both types of carriers (electrons and hole) may be involved in the charge transport mechanism or additional scattering phenomenon may contribute to thermopower. Because no current flows, the thermopower does not depend on the connectivity of conducting regions, and the thermopower of individual grains are additive. There have been many measurements of the thermopower of samples with $x \approx 0.3$ which exhibit a metal-insulator transition. These data, on ceramics, thin films and single crystals, are not very consistent and results are sensitive to details of sample preparation and composition (Jaime etal., 1996; Mahendiran et al., 1996b; Mandal 2000).

3.4.1 Low temperature behavior ($T<T_P$)

Most of the studies on thermopower were reported on the manganites with varying doping concentration [Battacharya et al., 2003; Jirak et al., 1985; Mahendiran et al., 1996b; Volger 1954). In order to get further insight into the effect of particle size on thermopower, the variations of thermopower as a function of sintering temperature on various manganites systems were carried out. This section describes thermopower results obtained by the authors of the present investigation on various manganite systems doped with both divalent and monovalent ions sintered at different temperatures. Figure 12 shows the variation of seebeck coefficient (S) with temperature in LCMO and NSMO manganites. It has been observed that the magnitude of S is found to increase with decreasing particle size and positive throughout the temperature range of investigation, thereby representing that the charge carriers are holes for LSMO, LBMO, NSMO, LNMO, LCMO-8, LCMO-9 and LCMO-10. In contrast to this, the sign of S for LCMO-11 changes from positive to negative value indicating the coexistence of two types of carriers. Banerjee et al., (2003) has also found a similar variation of S with varying particle size in lead doped manganites. One can notice from the figure that as the temperature of the samples is decreased from room temperature to liquid nitrogen temperature, S values increase continuously attaining a maximum value with a sharp peak in the vicinity of T_C. The peak observed at T_C may be attributed to enhancement in spin polarization caused by the magnetic transition (Das et al., 2004). Apart from this, except LCMO-8 and LCMO-9 all are found to exhibit a broad peak around 120 K and similar behavior was reported earlier (Das et al., 2004; Urushibara et al., 1995). It was reported earlier that (Banerjee et al., 2003) phonon drag (S_P) and magnon drag (S_M) contributions are present in the low temperature region and that these are proportional to their respective specific heat contribution so that $S_P \alpha T^3$ and $S_M \alpha T^{3/2}$. This suggests that in the low temperature ferromagnetic region, a magnon drag effect is produced due to the presence of electron - magnon interaction along with the phonon drag due to electron – phonon interaction.

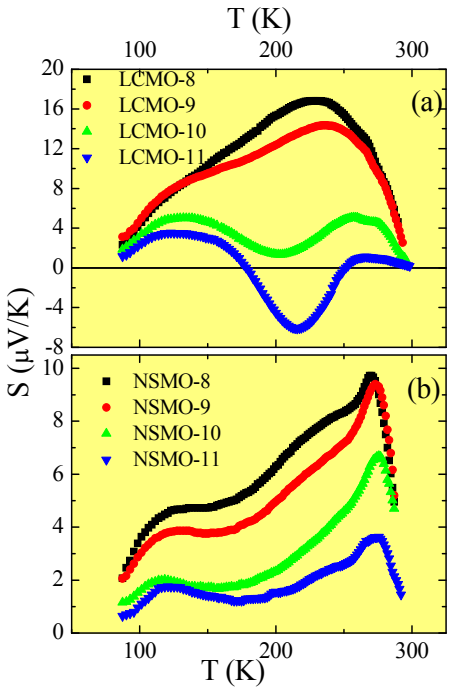

Fig. 12. Variation of seebeck coefficient (S) with temperature of LCMO & NSMO manganites.

In general, to understand the influence of various contributions to TEP in ferromagnetic region, the following equation was used earlier (Mandal 2000)

$$S = S_0 + S^{3/2}T^{3/2} + S_4T^4 \tag{2}$$

where S_0 term has no physical origin and is inserted to account for the problem of truncating the low temperature thermopower data. The second term of the equation represents the single-magnon scattering process. Although the origin of S_4T^4 term is still not clear, it is generally believed that it may be due to spin wave fluctuation. It has been observed that the eq. (2) doesn't fit the TEP data in the entire ferromagnetic region. Therefore, the above equation has been modified by taking into account the diffusion and phonon drag contributions and the equation is as follows, (Kim et al., 2008),

$$S = S_0 + S_1T + S^{3/2}T_{3/2} + S_3T^3 + S_4T^4 \tag{3}$$

Here, the second and fourth terms represents the diffusion and phonon drag contributions to TEP respectively. The experimental data in the low temperature region were fitted to the above equation and the solid curve in Figure 13 (a) (in the case of NSMO) represents the best fit to the experimental data in FMM region and the best fit parameters for NSMO sample is given in Table 1.

Sample code	S_0 (μV/K)	S_1 (μV/K²)	$S_{3/2}$ (μV/K^{5/2})	S_3 (μV/K⁴)	S_4 (μV/K⁵)	E_P (meV)	E_S (meV)	α′
NSMO-8	-62.936	2.3350	-0.1849	2.0×10^{-5}	-7.46×10^{-11}	140.99	30.56	-0.117
NSMO-9	-50.745	1.8982	-0.1505	2.0×10^{-5}	-5.84×10^{-11}	130.92	21.35	-0.107
NSMO-10	-38.148	1.3672	-0.1071	1.0×10^{-5}	-3.59×10^{-11}	125.95	17.60	-0.065
NSMO-11	-29.817	1.1270	-0.0897	0.8×10^{-5}	-3.13×10^{-11}	118.83	12.12	-0.047

Table 1. The best fit parameters obtained from thermoelectric power data for NSMO system (EP & ES represent the activation energies obtained from resistivity and thermopower data)

All the fitting parameters decrease with increasing particle size. This might be due to the magnetic domain and grain boundary scattering mechanism discussed previously in analyzing resistivity data of the samples.

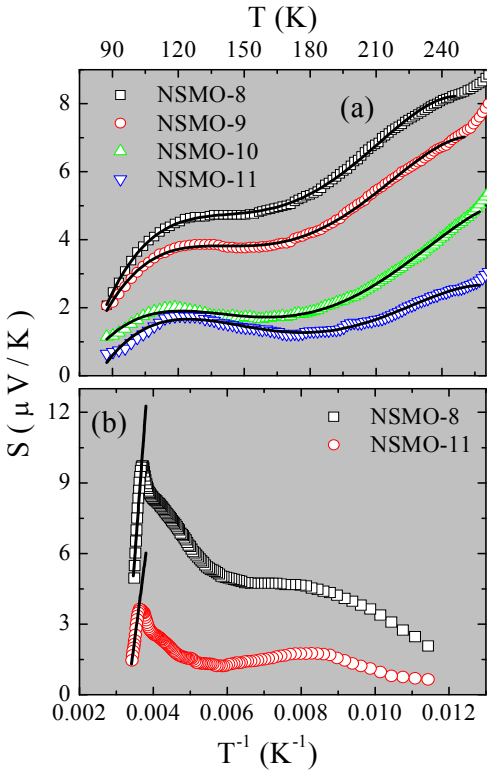

Fig. 13. (a) The temperature dependence of TEP of NSMO group of samples. The solid line represents the fitting with eq (3). (b) Variation of S vs $T^{-1}(K^{-1})$ of NSMO manganites. The solid line represents the best fit to the small polaron hopping model.

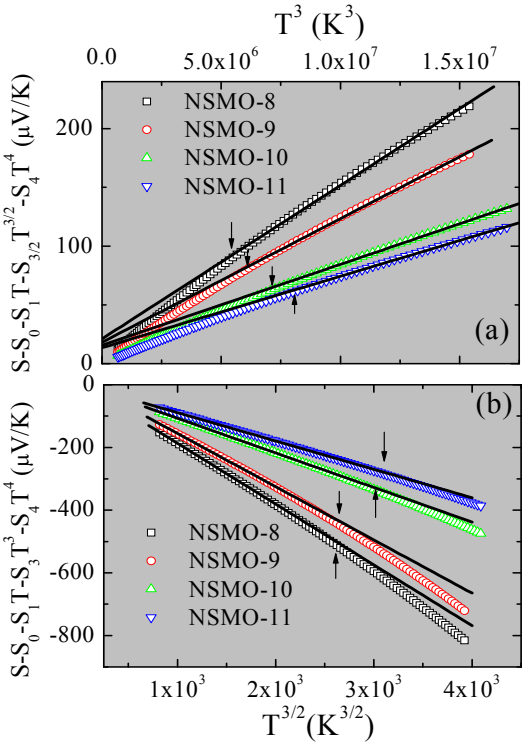

Fig. 14. (a) Variation in phonon drag component with T^3 and (b) variation in magnon drag component with $T^{3/2}$. The arrow marks represents the deviation of linear fit to the data.

In order to explain the origin of peak at low temperatures, the phonon and magnon drag contributions to the TEP were investigated using eq. (3). The variation of phonon drag component with T^3 for all the samples is shown in Figure 14 (a). It is clear from the figure that the phonon drag contribution (S_3T^3) is found to vary linearly up to a certain temperature and deviates (indicated by arrow in the figure) below 250K. As the phonon drag contribution deviates at 250K, it has been concluded that the origin of the low temperature peak might not be due to the phonon drag effect. It is interesting to note from Fig. 14(a) that the extrapolated phonon drag component is approaching zero as the sample approaches to T = 0 indicating that the phonon drag effect might be disappearing probably due to depleting number of phonons at T = 0. It can also be seen from the figure that the deviation temperatures occurring from phonon and magnon drag are almost equal in the case of NSMO-8 and NSMO-9 samples indicating that the magnon and phonon drag effects are occurring in different temperature regions. The magnon drag component was calculated from eq (3) and is shown in Figure 14(b). It is interesting to note that the magnon drag component fits well below 200K, indicating that the low temperature peak might have arisen due to magnon drag effect (Venkataiah & Reddy, 2009b).

3.4.2 High temperature behavior ($T>T_P$)

The charge carriers in the insulating region are not itinerant and the transport properties are governed by thermally activated carriers because the effect of Jahn-Teller distortions in manganites results in strong electron-phonon coupling and hence the formation of polarons. Therefore, the thermoelectric power data of the present samples in the insulating regime are fitted to Mott's polaron hopping equation,

$$S(T) = \frac{k_B}{e}\left[\frac{E_S}{k_B T} + \alpha\right] \tag{4}$$

where *e* is the electronic charge; E_S is the activation energy obtained from TEP data and α is a constant. α<1 implies the applicability of small polaron hopping model whereas α>2 is for large polaron hopping (Das et al., 2004). It has been found that the above equation fits well with the experimental data of the present investigation. The best fit curves of S versus 1/T of NSMO samples are shown in Figure 13(b). The calculated values of α for the samples of the present investigation are less than one, therefore it may be concluded that the small polaron hopping mechanism is more appropriate to explain the thermopower data in the high-temperature regime.

3.5 Magnetoresistance

One of the important properties of the doped perovskite manganites is their mangetoresistace (MR).The percentage of MR is defined as the relative change in the electrical resistivity of a material on the application of an external magnetic field and is given by a relation,

$$MR\% = \frac{\rho_H - \rho_0}{\rho_0} X100 \tag{5}$$

where ρ_H and ρ_0 are the resistivities at a given temperature in the applied and zero magnetic fields, respectively. MR can be positive or negative depending on increase or decrease in the resistivity values. The magneto resistance studies were undertaken on all the five groups of samples of present investigation. The variation of electrical resisitivity with temperature at different fields for LBMO sample sintered at two different sintering temperatures (T_S = 800 & 1100^{o}C) is shown in Figure 15. It is also clear from the figures that the resistivity value decrease with increasing magnetic field and T_P shifts towards high temperature side. This may be due to the fact that the applied magnetic field induces delocalization of charge carriers, which in turn might suppress the resistivity and also causes the local ordering of the magnetic spins. Due to this ordering, the ferromagnetic metallic (FMM) state may suppress the paramagnetic insulating (PMI) regime. As a result value of T_P shifts to high temperature with application of magnetic field. The variation of MR% with temperature in the case of LBMO system is shown in Figure 16.The measurements of MR reveal that the maximum MR is observed for the samples sintered at the lowest temperature. All the samples are exhibiting high MR% at low magnetic fields and also remain high in low temperature regime and then decrease with increasing temperature. This is a clear signature of low field magnetoresistance (LFMR) behavior.

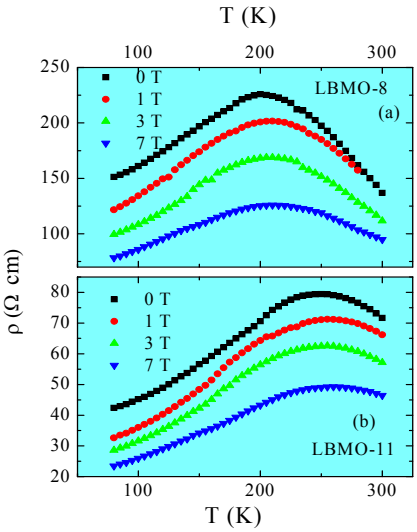

Fig. 15. ρ-T plots of (a) LBMO-8 &(b) LBMO-11 manganites at different magnetic fields.

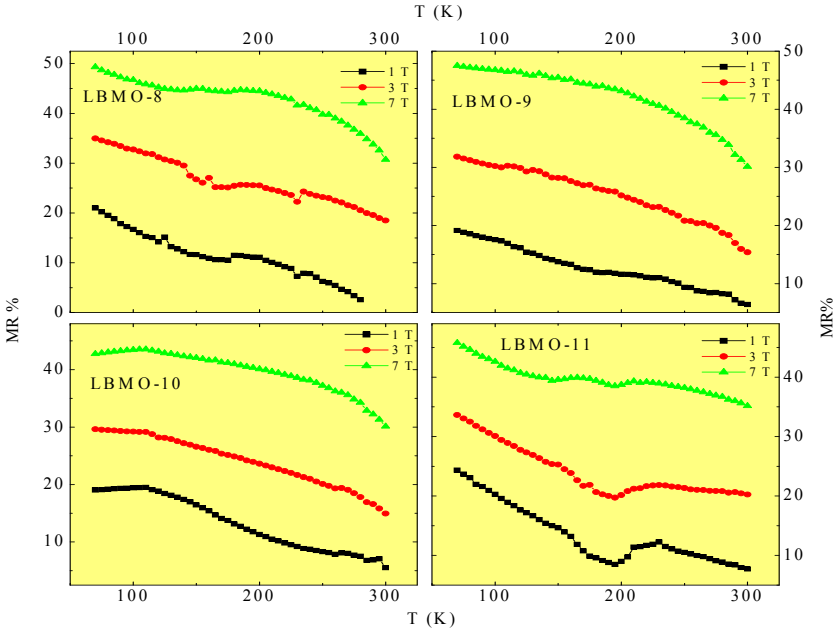

Fig. 16. Variation of MR% with temperature at different magnetic fields for LBMO group of manganites.

The observed behavior may be explained on the basis of a qualitative model. According to this model, magnetoresistance may be classified into two categories (Dutta et al., 2003; Hwang et al., 1996; Mandal et al., 1998). The first one is the intrinsic MR, which arises due to the suppression of spin fluctuations by aligning the spins on the application of magnetic field. This MR has highest value near the ferromagnetic transition temperature and is generally observed among single crystalline bulk as well as thin films. In the polycrystalline samples, there is an additional MR, which is extrinsic in nature; arises due to inter-grain spin-polarized tunneling (ISPT), across the grain boundaries (GBs). This MR contribution increases as the temperature decreases and is usually found in nanocrystalline materials. Rivas et al. (2000) pointed out that the sol–gel prepared samples sintered at low temperatures (900°C) with particle size less than 150nm show more extrinsic nature of magnetoresistance than the intrinsic one. Until recently, it was believed that the former mechanism is responsible for the MR at high fields and the later one at low fields. But recent experiments have shown that high field response is also due to the existence of GB. The nature of GB is a key ingredient in the mechanism of electrical transport, as it constitutes the barrier through which carriers cross or tunnel (Hsu et al., 2006). In view of this, one may conclude that the samples of the present investigation, might be exhibiting extrinsic nature of magnetoresistance arising due to inter-grain spin-polarized tunneling.

3.6 Conduction mechanism

Inspite of extensive experimental and theoretical work to understand the conduction mechanism of CMR materials in general and rare-earth manganites in particular, the present scenario is more confusing than earlier. Therefore, an effort has been made to understand the conduction mechanism of these materials by analyzing the experimental data of both the ferro-as well as the paramagnetic regions using various theoretical models.

3.6.1 Low temperature resistivity ($T<T_P$)

In order to understand the relative strengths of different scattering mechanisms originating from different contributions both as a function of particle size and magnetic field, the FMM ($T<T_P$) part of electrical resistivity data of the samples of the present investigation has been fitted to various empirical equations (De Teresa et al., 1996; Kubo & Ohata, 1972; Schiffer et al., 1995; Snyder et al., 1996; Urushibara et al., 1995). Except LCMO samples, the low temperature resistivity of LSMO, LBMO, NSMO and LNMO group of samples is found to fit well with the equation,

$$\rho = \rho_0 + \rho_2 T^2 + \rho_{4.5} T^{4.5} \tag{6}$$

where ρ_0 arises due to the grain or domain boundaries, $\rho_2 T^2$ indicates the electron–electron scattering, while $\rho_{4.5} T^{4.5}$ is attributed to two magnon scattering process. The two magnon process is more favorable in half-metallic band structure materials such as manganites. The best fit curve for a representative sample viz., LBMO sintered at 800 & 1100 °C various sintering temperatures is shown in Figure 17 (a, b) and fitting parameters are given in Table 2. On the other hand, in the case of LCMO system resistivity in metallic region is well fitted to an equation $\rho=\rho+\rho_{2.5}T^{2.5}$, the term $\rho_{2.5}T^{2.5}$ the resistivity due to single magnon scattering mechanism. It has been observed that the temperature independent residual resistivity term for all the samples is larger than that obtained for single crystals.

Sample code	ρ_0 (Ωcm)			ρ_2 (Ωcm K^{-2})			$\rho_{4.5}$ (Ωcm K$^{-4.5}$)		
	B=0T	B=3T	B=7T	B=0T	B=3T	B=7T	B=0T	B=3T	B=7T
LBMO-8	133.02	81.82	63.28	30.50×10^{-4}	28.60×10^{-4}	24.70×10^{-4}	12.20×10^{-9}	9.78×10^{-9}	7.62×10^{-9}
LBMO-9	88.95	59.47	46.47	28.10×10^{-4}	23.10×10^{-4}	21.10×10^{-4}	3.10×10^{-9}	1.98×10^{-9}	1.44×10^{-9}
LBMO-10	59.12	38.82	32.01	27.50×10^{-4}	22.00×10^{-4}	16.70×10^{-4}	2.00×10^{-9}	1.43×10^{-9}	1.08×10^{-9}
LBMO-11	36.28	21.86	18.95	10.20×10^{-4}	9.30×10^{-4}	7.30×10^{-4}	1.30×10^{-9}	3.01×10^{-10}	2.16×10^{-10}

Table 2. The best-fit parameters obtained from low temperature ($T<T_P$) resistivity data both in presence and in absence of magnetic field for LBMO group of mangnaites sintered at different temperatures.

Further, the fitting parameters are found to decrease continuously with increasing particle size as well as the magnetic field. One of the reasons may be due to decrease in the grain boundary size with increasing sintering temperature. The second reason may be due to the spins present in the domain wall align in the direction of applied magnetic field resulting in the enlargement of magnetic domains. Therefore, the parallel configuration of the spins present in the domain, suppresses various scattering contributions and as a result ρ_0, ρ_2, $\rho_{2.5}$ and $\rho_{4.5}$ are decreasing with the application of the magnetic field and sintering temperature. (Banerjee et al., 2001).

3.6.2 Insulating region ($T>T_P$)

The pair-density function (PDF) analysis (Toby & Egami, 1992; Mott & Davis 1971) of powder neutron scattering data on manganites shows that the high temperature semiconducting region ($T>T_P$) is mainly due to lattice polarons. The analysis clearly indicates that the doped holes in manganites are likely to be localized within one octahedron of Mn^{4+} ion, forming a single-site polaron (small polarons). These small polarons in the high temperature semi-conducting regime of electrical resistivity data are in good agreement with the theoretical prediction of entropic localizations. Therefore, an attempt has been made to fit the high temperature resistivity data of the samples of present investigation to small polaron hopping (SPH) model explained by the equation (Emin & Holstein 1969),

$$\rho = \rho_\alpha T \exp\left(\frac{E_\rho}{k_B T}\right) \tag{7}$$

where ρ_a is a pre-factor and E_ρ is the activation energy. $\rho_a = 2k_B/3ne^2a^2v$, where k_B is Boltzmann's constant, e is the electronic charge, n is the number of charge carriers, a is site – to – site hopping distance and v is the longitudinal optical phonon frequency.

The high temperature data of the samples of the present study is found to fit well with the SPH model. A typical plot of ln (ρ/T) versus T^{-1} in the case of LBMO-8 & 11 is shown in Figure 17 (c, d). From the best fit parameters the activation energy (Eρ) values have been estimated and the values are found to decrease continuously with increasing particle size and magnetic field. The observed behavior may be due to the fact that the increasing particle size may increase the interconnectivity between grains, which in turn enhances the possibility

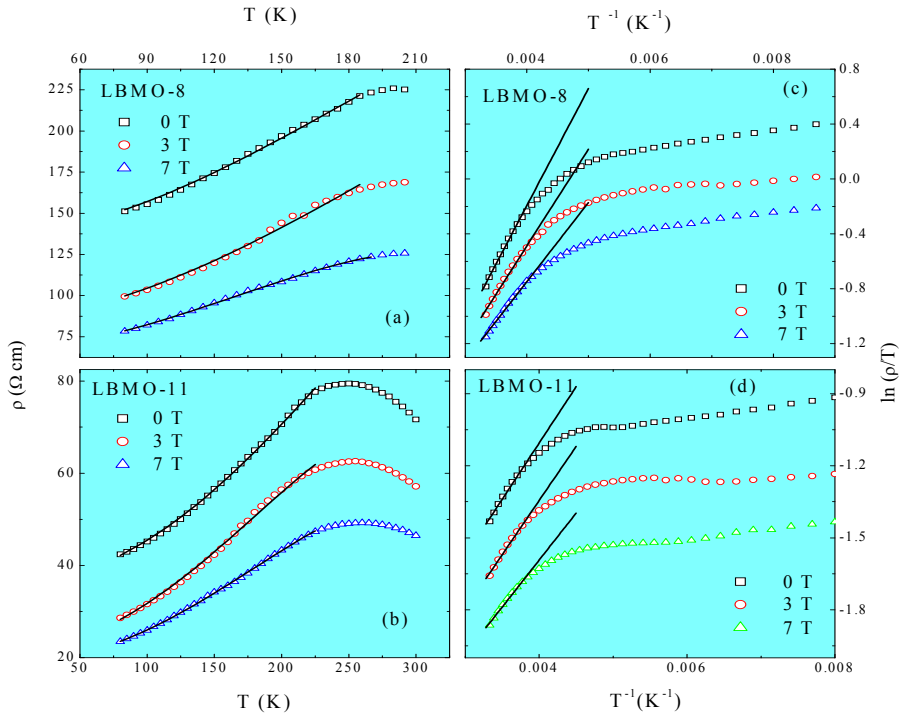

Fig. 17. (a,b) ρ-T plots of LBMO manganites sintered at 800 & 1100°C both in presence and absence of magnetic field. The solid line gives the best-fit to eq.(6) and (c,d) plots of ln(ρ/T) vs. T^{-1} (K^{-1}) in LBMO-8 & LBMO-11 samples. The solid line indicates the best fit to SPH model.

of conduction electron to hop to the neighboring sites, thereby conduction bandwidth increases and as a result the value of Eρ decreases. Therefore, the conduction bandwidth of the materials may be modified by proper tuning of their particle size. The increase in Eρ in the presence of magnetic field is mostly attributed to the increase of charge localization (Banerjee et al., 2002).

4. Summary and outlook

For over more than a decade, studies on manganites have been focused on both various details covering the underlying fundamental Physics and on applied aspects; it is the former which has received most of the attention. This chapter embodies the influence of sintering temperature on physical properties in doped manganites. Five series of doped manganties i.e., $La_{0.67}Ca_{0.33}MnO_3$, $La_{0.67}Sr_{0.33}MnO_3$, $La_{0.67}Ba_{0.33}MnO_3$, $Nd_{0.67}Sr_{0.33}MnO_3$ and $La_{0.67}Na_{0.33}MnO_3$, were synthesized using sol-gel method by sintering the samples at four different temperatures. The crystallite sizes of all the samples are in the nanometer range

and are found to decrease on lowering the sintering temperature. The ferro to paramagnetic transition temperatures (T_C) remains unaltered, while the metal to insulator transitions (T_P) decrease with decreasing sintering temperature. The behavior was explained using core-shell model. The percentage of magentoresistance is high at low temperatures and varies linearly with decreasing temperature and the behavior is explained based on inter grain spin polarized tunneling mechanism. The Seebeck coefficient decreases with increasing sintering temperature and remains positive throughout the temperature range of investigation indicating that the charge carriers are holes. The broad peak observed in the low temperature thermopower data was analyzed using phonon and magnon drag terms and it has been concluded that magnon drag contribution dominates in the low temperature region. The resistivity data in the low temperature region were analyzed using various theoretical models. The contribution from various scattering mechanism are found to depend both on grain size and applied magnetic field. Small polaron hopping mechanism dominates both the resistivity and thermopower data in the high temperature region.

The trends of sintering effects on various physical properties, particularly the electric and magnetic transition temperatures are encouraging. The authors envisage that further work will be useful in achieving one of the challenging aspects such as the above room temperature ferromagnetism in these highly spin polarized half metallic manganites for future commercial spintronic devices.

5. Acknowledgments

The authors acknowledge Defence Research and Development Organisation (DRDO) for funding the part of the work. The authors also thank Dept. of Science & Technology, Govt. of India for assisting part of the work. One of the authors (YKL) thanks Council of Scientific and Industrial Research (CSIR), Govt. of India for sanctioning the fellowship.

6. References

Banerjee A, S. Pal, B.K. Chaudhuri, (2001). Nature of small-polaron hopping conduction and the effect of Cr doping on the transport properties of rare-earth manganite $La_{0.5}Pb_{0.5}Mn_{1-x}Cr_xO_3$. *J. Chem. Phys.* 115, 1550.

Banerjee A, S. Pal, S. Bhattacharya, B.K. Chaudhuri, (2002) Particle size and magnetic field dependent resistivity and thermoelectric power of $La_{0.5}Pb_{0.5}MnO_3$ above and below metal-insulator transition. *J. Appl. Phys.* 91, 5125.

Balcells L I, J Fontcuberta, B Martinez and X Obradors (1998) High-field magnetoresistance at interfaces in manganese perovskites. *Phys. Rev. B* 58, R14697

Battacharya S, S Pal, A. Banerjee, H. D. Yang, and B. K. Chaudhuri, (2003). Magnetotransport properties of alkali metal doped La-Ca-Mn-O system under pulsed magnetic field: Decrease of small polaron coupling constant and melting of polarons in the high temperature phase. *J.Chem. Phys.* 119, 3972

Das S, A. Poddar, B. Roy, and S. Giri, (2004). Studies of transport and magnetic properties of Ce-doped $LaMnO_3$. *J. Alloys Compd.* 365, 94

Dey P and Nath T.K (2006), Effect of grain size modulation on the magneto-and electronic-transport properties of $La_{0.7}Ca_{0.3}MnO_3$ nanoparticles: The role of spin-polarized tunneling at the enhanced grain surface. *Phys. Rev. B* 73, 214425

De Teresa J. M, M. R. Ibarra, J. Blasco, J. Garcia, C. Marquina and P A Algarabel (1996). Spontaneous behavior and magnetic field and pressure effects on $La_{2/3}Ca_{1/3}MnO_3$ perovskite. *Phys. Rev. B* 54, 1187

Dutta A, N. Gayathri, R. Ranganathan, (2003). Effect of particle size on the magnetic and transport properties of $La_{0.875}Sr_{0.125}MnO_3$. *Phys. Rev. B* 68, 054432

Dogotto E (2003). *Nanoscale Phase Separation and Colossal Magnetoresistance* Springer Series in Solid State Physics vol 136

Emin D, T. Holstein, (1969). Studies of small-polaron motion IV. Adiabatic theory of the hall effect. *Ann. Phys.* 53, 439

Fu Y (2000). Grain-boundary effects on the electrical resistivity and the ferromagnetic transition temperature of $La_{0.8}Ca_{0.2}MnO_3$. *Appl. Phys. Lett.* 77, 118

Goldschmidt V (1958). *Geochemistry* (Oxford: Oxford University Press)

Goodenough J B (2003). Rare earth manganese perovskites Handbook on the Physics and Chemistry of Rare Earth vol 33 ed KA Gschneidner Jr et al Amsterdam: Elsevier

Gaur A and Verma G. D. (2006). Sintering temperature effect on electrical transport and magnetoresistance of nanophasic $La_{0.67}Sr_{0.33}MnO_3$. *J. Phys.: Condens. Matter* 18, 8837

Hueso L. E, F. Rivadulla, R.D. Sanchez, D. Caeiro, C. Jardon, C. Vazquez-Vazquez, J. Rivas, M.A. Lopez-Quintela, (1998). Influence of the grain-size and oxygen stoichiometry on magnetic and transport properties of polycrystalline $La_{0.67}Ca_{0.33}MnO_{3\pm\delta}$ perovskites. *J. Magn. Magn. Mater.* 189, 321

Hsu C.Y, H. Chou, B.Y. Liao, J.C.A. Huang, (2006). Interfacial and quantum wall effects on ac magnetotranport of $La_{0.67}Sr_{0.33}MnO_3/La_{1.4}Sr_{1.6}Mn_2O_7$ composites. *Appl. Phys. Lett.* 89, 262510.

Hwang H. Y, S. W. Cheong, N. P. Ong, and B. Batlogg, (1996). Spin-polarized intergrain tunneling in $La_{2/3}Sr_{1/3}MnO_3$. *Phys. Rev. Lett.*77, 2041.

Hwang H. Y, S-W. Cheong, P. G. Radaelli, M. Marezio, and B. Batlogg, (1995). Lattice effects on the magneoresistance oin doped $LaMnO_3$. *Phys. Rev. Lett.* 75, 914.

Jirak, Z., Krupicka, S., Simsa, Z., Dlouha, M., and Vratislav, S., (1985). Neutron diffraction study of $Pr_{1-x}Ca_xMnO_3$ perovskites. *J. Magn. Magn. Mater.* , 53, 153

Jaime M, M.B. Salamon and K. Pettit et al., (1996). Magnetothermopower in $La_{0.67}Ca_{0.33}MnO_3$ thin films. *Appl. Phys. Lett.* 68, 1576

Kubo K & N. Ohata, (1972). A quantum theory of double exchange. *J. Phys. Soc. Japan,* 33, 21

Kwon C. W, M. C. Robson, K-C. Kim, J. Y. Gu, S. E. Lofland, S.M. Bhagat, Z. Trajanovic, M. Rajeswari, T. Venkatesan, A. R. Kratz, R. D. Gomez, and R. Ramesh, (1997). Stress-induced effects on epitaxial $(La_{0.7}Sr_{0.3})MnO_3$ films. *J. Magn. Magn. Mater.*172, 229.

Kim B. H, J. S. Kim, T. H. Park, D. S. Le, and Y. W. Park, (2008). Magnon drag effect as the dominant contribution to the thermopowe in $Bi_{0.5-x}La_xSr_{0.5}MnO_3$ ($0.1\leq x\leq 0.4$). *J. Appl. Phys.*103, 113717

Kalyana Lakshmi Y, G. Venkataiah, M. Vithal and P. Venugopal Reddy (2008). Magnetic and electrical behavior of $La_{1-x}A_xMnO3$ (A= Li, Na, K and Rb) manganites. *Physica B*. 430, 3059

a Kalyana Lakshmi Y and P. Venugopal Reddy, (2009). Influence of sintering temperature and oxygen stoichiometry on electrical transport properties of $La_{0.67}Na_{0.33}MnO_3$ manganites. *J. Alloys Compd*. 470, 67

b Kalyana Lakshmi Y and P. Venugopal Reddy, (2009). Electrical behavior of some silver-doped lanthanum-based CMR materials. *J. Magn. Magn. Mater*. 321, 1240

Kalyana Lakshmi Y, G. Venkataiah and P. Venugopal Reddy, (2009). Magnetoelectric behavior of sodium doped lanthanum manganites. *J. Appl. Phys.* 106, 023707

Kalyana Lakshmi Y and P. Venugopal Reddy (2010). Influence of silver doping on the electrical and magnetic behavior of $La_{0.67}Ca_{0.3}MnO_3$ manganites. *Solid State Sciences* 12, 1731

Kalyana Lakshmi Y and P. Venugopal Reddy, (2011). Investigation of ground state in sodium doped neodymium manganites. *Phys. Lett. A* 375, 1543

Mahesh R, Mahendiran R, Raychaudhuri A K and Rao C N R (1996). Effect of particle size on the gaint magnetoresistance of $La_{0.67}Ca_{0.33}MnO_3$. *Appl. Phys. Lett.* 68, 2291

Malavasi M, M.C.Mozzati, C.B. Azzoni, G. Chiodelli, G. Flor,(2002). Role of oxygen content on the transport and magnetic properties of $La_{1-x}Ca_xMnO_{3\pm\delta}$ manganites. *Solid State Commun.*123 321.

a Malavasi L, M. C. Mozzati, S. Polizzi, C. B. Azzoni, and G. Flor, (2003). Nanosized sodium-doped lanthanum manganites: Role of the synthetic route on their physical properties. *Chem.Mater.* 15, 5036

b Malavasi L, M. C. Mozzati, C. Tealdi, C. B. Azzoni and G. Flor. (2005). Influence of Ru doping on the structure, defect chemistry, magnetic interaction, and carrier motion of the $La_{1-x}Na_xMnO_{3+\delta}$. *J. Phys. Chem. B*, 109, 20707.

a Mahendiran, R., Tiwary, S., Raychaudhuri, A.,Mahesh, R., and Rao, C. N. R.,(1996). Thermopower and nature of the hole-doped states in $LaMnO_3$ and related systems showing gaint magnetoresistance. *Phys. Rev. B* 54, R9604.

b Mahendiran, R., R Mahesh, N Rangavittal, S Tewari, A K Raychauduri, T V Ramakrishnan and CNR Rao, (1996). Structure, electron-transport properties, and gaint magnetoresistance of hole-doped $LaMnO_3$ systems. *Phys. Rev. B* 53, 3348.

Mandal P (2000). Temperature and doping dependence of the thermopower in $LaMnO_3$. *Phys. Rev. B* 61, 14675

Mandal P, K. Barner, L. Haupt, A. Poddar, R. von Helmolt, A. G. M.Jansen, and P. Wyder, (1998). High-field magnetotranport properties of $La_{2/3}Sr_{1/3}MnO_3$ and $Nd_{2/3}Sr_{1/3}MnO_3$ systems. *Phys. Rev. B* 57, 10256

Millis A J, Littlewood P B and Shraiman B (1995). Double exchange alone does not explain the resistivity of $La_{1-x}Sr_xMnO_3$. *Phys. Rev. Lett.* 74, 5144

Mott N F, E.A. Davis, (1971). Electronic Process in Noncrystalline Materials,Clarendon, Oxford,.

Okuda T, A. Asamitsu, Y. Tomioka, T. Kimura, Y. Taguchi, and Y. Tokura, (1998). Critical behavior of the metal-insulator transition in $La_{1-x}Sr_xMnO_3$. *Phys. Rev. Lett.* 81, 3203

Ramirez A. P. (1997). Colossal magnetoresistance. *J. Phys.:Condens. Matter* 9, 8171

Rao R. A, D. Lavric, T. K. Nath, C. B. Eom, L. Wu, and F. Tsui,(1998) Three-dimensional strain states and crystallographic domain structures of epitaxial colossal magnetoresistive $La_{0.8}Ca_{0.2}MnO_3$ thin films. *Appl. Phys. Lett.* 73, 3294

Rivas J, L.E. Hueso, A. Fondado, F. Rivadulla, M.A. Lopez-Quintela, (2000). Low field magnetoresistance effects in fine particles of $La_{0.67}Ca_{0.33}MnO_3$ perovskites. *J. Magn.Magn. Mater.* 221, 57.

Schiffer P, A. Ramirez, W. Bao & S.-W. Cheong, (1995). Low temperature magnetoresistance and the magnetic phase diagram of $La_{1-x}Ca_xMnO_3$. *Phys. Rev. Lett.* 75, 3336

Shankar K. S, S. Kar, G.N. Subbanna, A.K. Raychaudhuri, (2004) Enhanced ferromagnetic transition temperature in nanocrystalline lanthanum calcium manganese oxide ($La_{0.67}Ca_{0.33}MnO_3$). *Solid State Commun*. 129, 479.

Suzuki Y, H. Y. Hwang, S. W. Cheong, and R. B. vanDover, (1997). The role of strain in magnetic anisotropy of manganite thin films. *Appl. Phys. Lett.* 71, 140

Snyder G.J, R.Hiskes, S.Dicarolis, M.Beasley & T.Geballe, (1996). Intrinsic electrical transport and magnetic properties of $La_{0.67}Ca_{0.33}MnO_3$ and $La_{0.67}Sr_{0.33}MnO_3$ MOCVD thin films. *Phys. Rev.B* 53, 14434

Toby B. H, T. Egami, (1992). Accuracy of pair distribution fuction analysis applied to crystalline and non-crystalline materials. *Acta Crystallogr. Sect. A* 48, 336.

Tokura Y (2000). *Colossal Magnetoresistive Oxides*, (Gordon and Breach,New York)

Urushibara A, Y. Moritomo, T. Arima, A. Asamitsu, G. Kido & Y. Tokura (1995). Insulator-metal transition and giant magnetoresistance in $La_{1-x}Sr_xMnO_3$. *Phys. Rev. B* 51, 14103

Volger, J., (1954). Physica, 20, 49

Venkataiah G, D. C. Krishna, M. Vithal, S. S. Rao, S. V. Bhat, V. Prasad, S. V. Subramanyam and P. Venugopal Reddy (2005). Effect of sintering temperature on electrical transport properties of $La_{0.67}Ca_{0.33}MnO_3$. *Physica B* 357, 370.

Venkataiah G and P. Venugopal Reddy, (2005). Electrical behavior of sol-gel prepared $Nd_{0.67}Sr_{0.33}MnO_3$.manganite system. *J. Magn. Magn. Mater*. 285, 343

a Venkataiah G, Y. Kalyana Lakshmi and P. Venugopal Reddy, (2007). Influence of particle size on electrical transport properties of $La_{0.67}Sr_{0.33}MnO_3$ manganite system. *J. Nanosci. Nanotech*. 7, 2000

b Venkataiah G, Y. Kalyana Lakshmi and P. Venugopal Reddy, (2007). Thermopower studies of $Pr_{0.67}Ca_{0.33}MnO_3$. manganite system. *J. Phys. D: Appl. Phys.* 40, 721

c Venkataiah G, V. Prasad and P. Venugopal Reddy, (2007). Anomalous variation of magnetoresistance in $Nd_{0.67-y}$ $Eu_ySr_{0.33}MnO_3$ manganites. *Solid State Commun.* 141, 73.

Venkataiah G, Y. K. Lakshmi and P. Venugopal Reddy, (2008). Influence of sintering temperature on resistivity, magnetoresistance and thermopower of $La_{0.67}Ca_{0.33}MnO_3$. *PMC Phys B* 1754, 1:7

a Venkataiah G and P. Venugopal Reddy, (2009). Variation of thermopower with crystallite size of $La_{0.67}Sr_{0.33}MnO_3$ manganites. *Phase Transitions* 82, 156

b Venkataiah G and P. Venugopal Reddy, (2009). Magnon drag contribution to thermopowe of $Nd_{0.67}Sr_{0.33}MnO_3$ nanocrystalline manganites. *J. Appl. Phys.* 106, 033706

Venkataiah G, J. C. A. Huang and P. Venugopal Reddy, (2010). Low temperature resistivity minimum and its correlation with magnetoresistance in $La_{0.67}Ba_{0.33}MnO_3$. nanomanganites. *J. Magn. Magn. Mater.* 322, 417

Vogel A. I, A text book of Quantitative Inorganic Analysis including Elementary Instrumental Analysis, (1978) 4th edn., Longman, London,.

Williamson G. K and W. H. Hall, (1953). X-ray line broadening from field aluminium and wolfram. *Acta Metall.* 1, 22.

Zhou J.-S, J. B. Goodenough, A. Asamitsu, and Y. Tokura, (1997). Pressure induced polaronic to itinerant electronic transition in $La_{1-x}Sr_xMnO_3$ crystals. *Phys. Rev. Lett.* 79, 3234

Zhang N, Ding W, Zhong W, Xing D and Du Y (1997). Tunnel-type gian magnetoresistance in the granular perovskite $La_{0.85}Sr_{0.15}MnO_3$. *Phys.Rev. B* 56, 8138

Zenar C, (1951). Interaction between the d-shell in the transition metals. II. Ferromagnetic compounds of manganese with perovskite structure. *Phys. Rev.* 82, 403.

Sintering - Methods and Products

Edited by Dr. Volodymyr Shatokha

ISBN 978-953-51-0371-4
Hard cover, 316 pages
Publisher InTech
Published online 23, March, 2012
Published in print edition March, 2012

This book is addressed to a large and multidisciplinary audience of researchers and students dealing with or interested in sintering. Though commonly known as a method for production of objects from fines or powders, sintering is a very complex physicochemical phenomenon. It is complex because it involves a number of phenomena exhibiting themselves in various heterogeneous material systems, in a wide temperature range, and in different physical states. It is multidisciplinary research area because understanding of sintering requires a broad knowledge - from solid state physics and fluid dynamics to thermodynamics and kinetics of chemical reactions. Finally, sintering is not only a phenomenon. As a material processing method, sintering embraces the wide group of technologies used to obtain such different products as for example iron ore agglomerate and luminescent powders. As a matter of fact, this publication is a rare opportunity to connect the researchers involved in different domains of sintering in a single book.

InTech Europe
University Campus STeP Ri
Slavka Krautzeka 83/A
51000 Rijeka, Croatia
Phone: +385 (51) 770 447
Fax: +385 (51) 686 166
www.intechopen.com

InTech China
Unit 405, Office Block, Hotel Equatorial Shanghai
No.65, Yan An Road (West), Shanghai, 200040, China
中国上海市延安西路65号上海国际贵都大饭店办公楼405单元
Phone: +86-21-62489820
Fax: +86-21-62489821